



Reversible plasticity shape memory effect in carbon nanotubes reinforced epoxy nanocomposites



R. Abishera, R. Velmurugan^{*}, K.V.Nagendra Gopal

^a Department of Aerospace Engineering, Indian Institute of Technology Madras, Chennai 600036, India

ARTICLE INFO

Article history:

Received 8 August 2016

Received in revised form

24 October 2016

Accepted 27 October 2016

Available online 5 November 2016

Keywords:

Carbon nanotubes

Smart materials

Plastic deformation

Thermomechanical properties

Stress relaxation

ABSTRACT

Reversible plasticity shape memory (RPSM) property of multi-walled-carbon-nanotube (MWCNT) reinforced epoxy nanocomposites is investigated as an alternative to conventional shape memory programming and for possible applications in self-healing systems. A commercially available structural grade epoxy resin is tailored to realize RPSM effect and the material properties are further enhanced with the addition of MWCNT in the polymer matrix. The samples are characterized for their mechanical, thermal, morphological and crystallographic properties. This paper systematically investigates the effect of MWCNT addition on the properties of the epoxy matrix. To study the RPSM effect, the nanocomposites are programmed by cold drawing and stress relaxation below the glass transition temperature (T_g) and recovered by reheating above T_g . A comprehensive study on the effect of programming conditions like strain rate, strain level and stress relaxation time on the RPSM property is presented. Results reveal that all samples show excellent shape recovery property under various programming conditions. The addition of MWCNT resulted in a significant increase in modulus and strength, decrease in failure strain, increase in T_g and an improvement in RPSM properties like shape fixity, response temperature and recovery speed. As a result, this study shows that by controlling the parameters like glass transition temperature, filler content and the programming conditions, the material can be effectively designed for application in smart structures with shape memory and/or self healing capabilities.

© 2016 Elsevier Ltd. All rights reserved.

1. Introduction

Shape Memory Polymers (SMPs) are smart materials which can be programmed to hold a temporary shape under certain environmental conditions and revert back to its original shape on application of suitable external stimulus [1]. SMPs have been designed to respond to various stimuli like temperature change, light, electricity, solvent, change in pH, etc [2,3]. Conventionally a thermo-mechanical cycle of a thermally activated SMP involves a programming step and a recovery step. In the programming step, the SMP is deformed at a temperature above the glass transition (T_g) and subsequently cooled below T_g while holding the deformation to fix a temporary shape. The recovery step involves reheating the SMP above T_g to recover the original shape. Contrary to the conventional method, in order to realize Reversible plasticity shape memory (RPSM) effect, a modified programming step is employed wherein the temporary shape can be fixed by plastically

deforming the material at a temperature lower than T_g . This modified approach offers several advantages over the conventional approach like simplified programming step, improved recovery stress, faster recovery rate and higher recovery ratios [4,5]. It is to be noted that RPSM effect can be realized only when the material is deformed within a limit where no permanent defects like cracks occur and above the elastic limit (yield point) where there is plastic deformation. Another major drawback is low shape fixity due to the instantaneous recovery of elastic deformation. The effect of deformation temperature (T_d) on the mechanical and shape memory properties have been studied by several researchers. Gall and co-workers [6,7] showed that the failure strain is maximum when T_d is at the onset of the glass transition rather than above T_g . They also showed an improved recovery stress and recovery time when T_d is less than T_g . Feldkamp and Rousseau [8] studied the effect of T_d on epoxy based SMP and showed that the failure strain increased by five times at the onset of T_g . Lakhera et al. [9] studied an acrylate based SMP and observed a peak near the vicinity of T_g during constrained stress recovery for samples programmed at a temperature below T_g which was not observed for samples programmed at

^{*} Corresponding author.

E-mail address: ramanv@iitm.ac.in (R. Velmurugan).

temperatures above T_g . Thereby showing that the recovery stress in cold programmed SMP is higher than that of SMP programmed at temperatures above T_g . Hence from the above studies it can be concluded that the glass transition region must be ideally in the vicinity of room temperature in order to realize RPSM at large plastic strains. The effect of stress relaxation on the shape fixity by programming under cold-compression was studied by Li and Xu [10]. They used a polystyrene based SMP to show that the shape fixity increased (>90%) with the increase in relaxation time. The term “RPSM” first appeared in the work of Rodriguez et al. [11] where they used a combination of a cross-linked network polymer with a linear polymer network to achieve shape memory assisted self-healing. The importance and distinction of RPSM effect were further emphasized in a review by Xie [4].

The ability to recover large plastic deformations by materials with RPSM properties has been applied in designing thermally activated self healing systems. Wornya et al. [12] performed nanoindentation tests on an acrylate based SMP and showed that the samples were able to completely heal the surface deformation when heated above T_g . Xiao et al. [13] developed graphene reinforced epoxy nanocomposites and studied the ability to heal surface scratches and observed that even with a very low volume percentage (0.0025%) of graphene the self-healing ability increased significantly. Li et al. [14] reinforced SMP fibers stretched at a temperature below T_g in a thermosetting polymer matrix and showed that the system was able to close wide cracks via localized heating. They also showed that increase in pre-strain increased the recovery stress which in turn improved the crack closing efficiency. A two-step bio-mimetic method was proposed by Li and coworkers [15,16] to seal and then heal the polymeric systems. The RPSM property assists in bringing the cracked surfaces together while the reinforced thermoplastic particles ensure healing at a molecular level. Previous studies show that, RPSM materials can effectively recover/heal large plastic deformations and surface defects and also assist in healing wide cracks by enabling crack-closure through a thermal trigger. It should be noted that the RPSM materials cannot heal wide cracks independently and require a secondary system to re-bond the cracked surfaces [14,15].

SMPs have exceptional properties like high recoverable strain, low cost, easy processing, etc. but, their low mechanical properties, low recovery stress, and inherent insulating properties limit their applications [17]. In order to improve these properties, various strategies have been adopted including reinforcing the polymer matrix with fillers ranging from macro to nano scale. Several studies [18–21] have shown that addition of various nano fillers can efficiently improve the properties of bulk polymer while maintaining the characteristic behavior of the matrix. Among them carbon nanotubes with their exceptional mechanical, thermal and electrical properties [22] have been found successful in improving the matrix properties while improving the shape memory property of the matrix [23–27]. Koerner et al. [28] used morthane, a polyurethane-based thermoplastic elastomer filled with CNT and studied the shape memory properties. When compared to neat elastomer, CNT filled elastomer showed a significant increase in mechanical properties and shape memory properties like recovery stress and shape fixity. They also showed that the CNT filled elastomer can be actuated electrically and by an infrared light source, whereas the pure polymer could be actuated only by heat. The addition of carbon nanotubes in the SMP matrix simultaneously improved mechanical, shape memory and conducting properties, thereby overcoming the drawbacks of SMPs. The improvement in conducting properties with the addition of MWCNT provides alternate actuating mechanism via electricity which offers several advantages over actuating through external heat [29–31].

In this paper a commercially available structural grade epoxy

resin was tailored to realize RPSM effect. MWCNT was added to the epoxy matrix with an objective to improve the mechanical and shape memory properties. The prepared nanocomposites were characterized for their mechanical, thermal, morphological, crystallographic and RPSM properties. A comprehensive study was systematically conducted on the effect of filler content and programming conditions like deformation level, stress relaxation time and strain rate on the RPSM properties and the results are discussed.

2. Experimental methods

2.1. Material selection and sample preparation

The epoxy resin used in this study was a Diglycidyl ether of bisphenol A (DGEBA-Araldite LY556) obtained from Huntsman, India. Neopentyl glycol diglycidyl ether (NGDE) and Poly(propylene glycol) bis(2-aminopropyl) ether (Jeffamine230) were obtained from TCI, India and Sigma-Aldrich, India respectively. High purity Multi-Walled-Carbon-Nanotubes were obtained from Reinste Nano Ventures Pvt. Ltd., India. All materials were used in as-received condition.

As mentioned earlier, to realize RPSM effect at large plastic strains the onset of glass transition region must ideally be in the vicinity of room temperature. The transition region of the epoxy based SMP was tuned by following the procedure proposed by Xie et al. [32]. They showed that by stoichiometrically introducing varying amount of flexible aliphatic epoxy chains (NGDE) in an amine (Jeffamine230) cured aromatic epoxy system (DGEBA) the glass transition temperature can be tuned precisely as per requirements. Steps followed in sample preparation are as follows: weighed amounts of DGEBA, NGDE and MWCNT were mixed using a mechanical stirrer at 1500 rpm for 4 h. After mixing, weighed amount of hardener (Jeffamine 230) was added to the mixture and stirred with the same setting for another 15 min. The weight ratio of DGEBA to NGDE to Jeffamine230 was stoichiometrically varied until the glass transition region (determined by DSC) was ideally in the vicinity immediately above the room temperature. The final weight ratio of DGEBA to NGDE to Jeffamine230 with the desired requirements was determined to be 3:2:2. It should be noted that, as per suppliers data, DGEBA (Araldite LY556) has a large viscosity of 11000 mPa s. Whereas, NGDE and Jeffamine230 have very low viscosities of about 20 and 5.5 mPa s respectively at 25 °C. The viscosity of the resultant mixture without any filler was 150 mPa s (measured using a Brookfield Rotational Viscometer). This low viscosity assists in easy dispersion of MWCNT and also in obtaining void-free samples. The mixture was poured into a dog-bone shaped (ASTM D630 Type IV) silicone mold and cured at room temperature for 18 h, de-molded and post cured at 80 °C for 2 h. Sample designation and composition is given in Table 1. To characterize the prepared materials, at least three samples were tested for each experiment.

2.2. Material characterization

2.2.1. Mechanical characterization

The tensile properties of the prepared nanocomposites were obtained using a UTM fitted with a thermal chamber of M/s Kalpak Instruments and Controls, India. To get a comprehensive understanding of the thermo-mechanical behavior, the effect of strain rate and temperature on the mechanical behavior was studied. The samples were tested at strain-rates of 0.00033, 0.0013 and 0.0033/s at room temperature. The samples were also tested at 27 °C, 55 °C and 80 °C at a constant strain rate of 0.0013/s to get the mechanical properties at elevated temperatures.

Table 1
Composition of different samples (phr is parts per hundred DGEBA-NGDE-Jeffamine230).

| Sample Name | DGEBA (g) | NGDE (g) | Jeffamine 230 (g) | MWCNT (phr) | MWCNT Weight (%) |
|-------------|-----------|----------|-------------------|-------------|------------------|
| E-0-CNT | 42.86 | 28.57 | 28.57 | 0 | 0 |
| E-0.5-CNT | 42.86 | 28.57 | 28.57 | 0.5 | 0.49 |
| E-1-CNT | 42.86 | 28.57 | 28.57 | 1 | 0.99 |
| E-1.5-CNT | 42.86 | 28.57 | 28.57 | 1.5 | 1.47 |
| E-2-CNT | 42.86 | 28.57 | 28.57 | 2 | 1.96 |

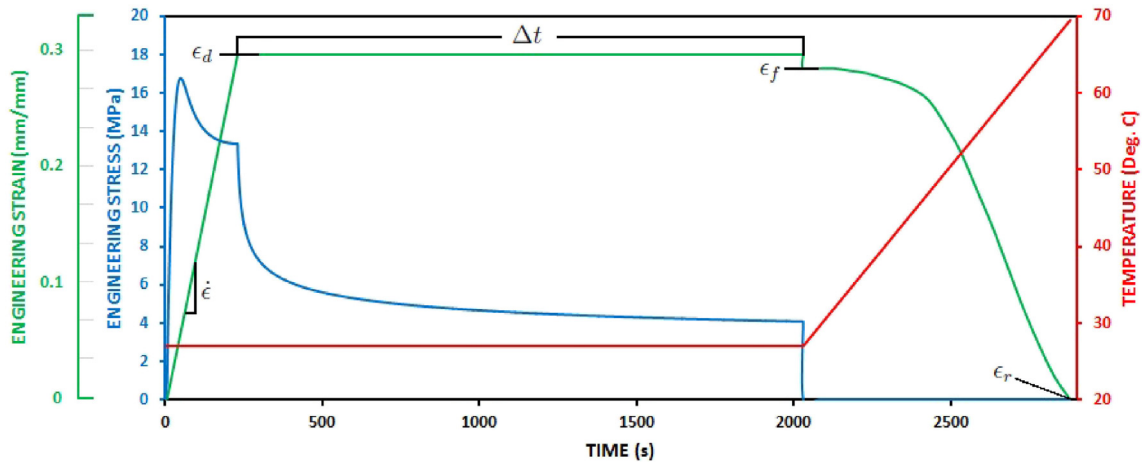


Fig. 1. Stress-Strain-Temperature history of a typical RPSM cycle.

2.2.2. Thermal characterization

The thermal properties were studied by using Differential Scanning Calorimeter (DSC) of M/s Netzsch DSC200 F3 Maia and a Push-Rod Dilatometer of M/s VB Ceramic Consultants, India. The DSC heating curves of all the samples were obtained for a temperature range from -30°C to 100°C in a nitrogen atmosphere. The heating rate was fixed at $10^{\circ}\text{C}/\text{min}$. Dilatometry tests were used to evaluate the linear thermal expansion properties.

2.2.3. Morphological characterization

Field Emission Scanning Electron Microscope (FESEM) of M/s FEI Quanta 3D FEG was used to study the morphology of the acquired MWCNTs. The fractured surfaces of the tensile specimens were also studied to evaluate the dispersion of MWCNT in the polymer matrix and the effect of MWCNT addition on tensile fracture.

2.2.4. Crystallographic characterization

The crystallographic nature of MWCNT and the prepared samples were evaluated by using a Bruker Discover D8 X-Ray Diffractometer (XRD). The 2θ range was chosen from 10° to 50° .

2.3. RPSM characterization

The following steps were followed to characterize the RPSM properties of a sample with ϕ phr of MWCNT and a gage length of L_0 : i) the sample was deformed at room temperature T_d to a specific strain ϵ_d at a constant strain rate $\dot{\epsilon}$, ii) the deformation was held at ϵ_d for a period of Δt to allow stress relaxation in the sample, iii) the sample was instantaneously unloaded and the fixed strain, ϵ_f was measured and finally, iv) the sample was heated to a temperature, T_r which was above the glass transition temperature at a heating rate of $\dot{T} = 3^{\circ}\text{C}/\text{min}$ under stress free conditions to study the strain recovery of the sample. An example of stress-strain-temperature history in an RPSM cycle is shown in Fig. 1. The effect of ϕ , ϵ_d , $\dot{\epsilon}$ and Δt on the RPSM properties were studied. The shape fixity (R_f)

and the shape recovery (R_r) were evaluated using the equations $R_f = \frac{\epsilon_f}{\epsilon_d} \times 100\%$ and $R_r = \frac{(\epsilon_f - \epsilon_r)}{\epsilon_f} \times 100\%$ respectively. ϵ_r is the residual strain after free recovery at T_r .

3. Results and discussions

3.1. Mechanical properties

Fig. 2 shows the effect of MWCNT addition on the tensile properties of epoxy nanocomposites under constant strain rate of

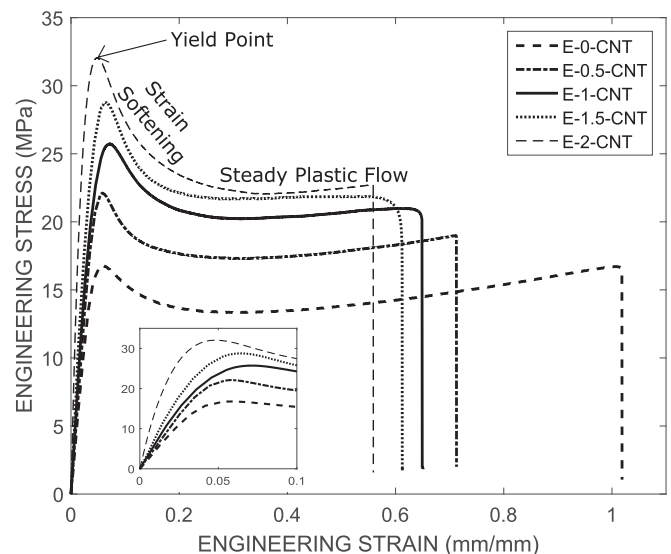


Fig. 2. Effect of MWCNT reinforcement on tensile properties. Inset: Enlarged image of the stress-strain curves showing the initial linear elastic region.

0.0013/s at room temperature (27 °C). The stress-strain curve of all the samples show the following regions: *i*) an initial linear portion indicating an elastic response, *ii*) the linear portion reaches a maximum point designating the yield point after which strain softening is observed which indicates neck formation. *iii*) Finally, there is a (nearly) constant stress region resulting from the propagation of the neck throughout the gage length culminating in failure.

It can be observed that addition of even a small amount of MWCNT (0.5 phr) results in a considerable increase in tensile modulus and yield strength indicating an effective reinforcement. The improvement in tensile properties is attributed to effective inter-facial load transfer between the filler and the matrix. From Table 2 it can be observed that further increase in MWCNT content leads to an increase in modulus and yield strength. After the yield point strain softening occurs due to a drop in inter-chain contributions to the stress [33–35]. It is observed that the strain softening is steeper in the nanocomposites when compared to pure epoxy (E-0-CNT). This trend increases with increase in MWCNT content suggesting that due to the collapse in inter-chain interactions there is a reduction in effective load transfer between the matrix and MWCNTs leading to steeper strain softening region in the stress-strain curve. A significant reduction in the failure strain is observed even with a small addition of MWCNT indicating a reduction in ductility with an increase in filler content. This can be attributed to the mismatch between matrix and filler properties especially in regions with agglomerations, which serve as stress concentration regions leading to failure. Further increase in MWCNT (i.e. >2 phr) drastically reduces the failure strain due to the increased filler agglomerations. From Fig. 2 and Table 2, it can be seen that nanocomposites with small filler content (upto 2 phr) exhibit qualitatively similar stress-strain curves with linearly-varying mechanical properties. For this reason and also for the sake of brevity here-on-forth the discussions are focused on neat epoxy and a representative nanocomposite (E-1-CNT).

Fig. 3 and Table 3 show the effect of strain rate at room temperature on neat epoxy and E-1-CNT. Strain rate had a qualitatively similar effect on all samples i.e. increase in strain rate increases the modulus and yield strength with a decrease in failure strain. Other important effect is steeper stress softening regime with the increase in strain-rate. The effect of strain rate on failure strain is more pronounced in nanocomposites when compared to that of pure epoxy [36]. Hence applying a high strain rate on nanocomposites with high filler content leads to failure at low strains. Though this might be considered as a drawback for high strain rate applications, it should be noted that for such applications T_g of the epoxy can be tailored further closer to room temperature thereby increasing the strain to failure at high strain rates.

Fig. 4 shows the effect of temperature at constant strain rate (0.0013/s) on pure epoxy and E-1-CNT. To avoid any relaxation effect the samples along with the grips were heated and held at the desired temperature for 30 min before beginning the test. The thermocouple was placed close to the samples, not on the sample so that the temperature must be considered as the temperature of air in the chamber. From Table 4 it can be seen that an increase in temperature causes a decrease in Young's modulus and yield strength with the samples showing a rubbery behavior at

temperatures well above T_g . Even at 55 °C the samples do not show a significant yield point for the tested strain rate. The reinforcement effect of MWCNTs can also be observed at temperatures above T_g . Figs. 3 and 4 show the well established fact that increase in strain rate and decrease in temperature have qualitatively similar effect on neat and filled epoxy.

3.2. Thermal properties

The shape memory transition temperature (T_g) is a critical parameter of a SMP [32]. The T_g is the temperature at which the thermally activated SMP gets activated i.e reverts back to original shape, which is an important parameter in designing smart structures. Hence, it is significant to understand any variation in T_g with MWCNT content. Fig. 5 gives the DSC thermo-graphs of various samples. All samples were tested at a constant heating rate of 10 °C/min in a nitrogen atmosphere from –30 °C to 100 °C. The glass transition temperatures were evaluated from the DSC curves with the aid of Netzsch-Proteus software version 6.1.0. The glass transition temperature of pure epoxy was found to be 42.1 °C. It should be noted that the high failure strain of the studied samples at room temperature is a result of the glass transition region being closer to room temperature. Table 5 shows the effect of MWCNT reinforcement on the glass transition region. It can be observed that, with the addition of MWCNT there is a gradual increase in the glass transition temperature. The effect of MWCNT on the glass transition temperature of the epoxy nanocomposite is still under extensive research with researchers reporting an increase, decrease or no change in T_g [37]. The studies have also shown that use of unmodified MWCNT directly in to the epoxy matrix resulted in an increase or no change in T_g . The glass transition region is characterized by an increase in mobility of the polymer chains. Introducing MWCNTs into the epoxy matrix might have reduced the mobility in the polymer chains resulting in an increase of T_g .

Table 5 gives the linear coefficient of thermal expansion (LCTE) of the studied samples above and below T_g obtained from dilatometry. The tests were conducted at two temperature ranges separately i.e. from 27 °C to T_g and from T_g to 70 °C and the slope of strain-temperature diagrams of the respective tests gave the LCTE below and above T_g . As shown in Table 5, all samples show a several fold increase in the LCTE at temperatures above T_g as compared to the LCTE at temperatures below T_g , a characteristic of amorphous polymers. At low filler content, MWCNT had little or no effect on LCTE both above and below the T_g . A considerable effect is observed in the sample reinforced with 2 phr MWCNT (E-2-CNT) where the LCTE decreases for both above and below T_g . This decrease may be attributed to low LCTE of the carbon nanotubes as reported in several studies [38,39].

3.3. Morphological properties

FESEM micro-graphs of pristine MWCNTs and fractured surface of unreinforced epoxy are shown in Fig. 6. The MWCNTs are found to be highly pure (>95% according to the supplier) with no visible impurities. The outer diameter is 20–40 nm with an average length of 7.5 μm yielding an average aspect ratio of 250. To evaluate the dispersion state and the degree of agglomerations the fractured

Table 2
Tensile performance of different samples.

| Property | E-0-CNT | E-0.5-CNT | E-1-CNT | E-1.5-CNT | E-2-CNT |
|------------------------|--|--|--|---|--|
| Modulus (MPa) | 450.23 ^{+13.7} _{-21.5} | 536.11 ^{+10.0} _{-17.3} | 616.21 ^{+34.0} _{-36.3} | 751.92 ^{+32.7} _{-5.3} | 867.80 ^{+38.7} _{-41.8} |
| Yield Strength (MPa) | 16.77 ^{+9.8} _{-1.8} | 22.11 ^{+1.3} _{-1.7} | 25.77 ^{+1.8} _{-1.1} | 28.76 ^{+1.1} _{-1.7} | 32.06 ^{+1.4} _{-1.6} |
| Failure-Strain (mm/mm) | 1.01 ^{+0.03} _{-0.03} | 0.71 ^{+0.09} _{-0.08} | 0.65 ^{+0.10} _{-0.02} | 0.61 ^{+0.02} _{-0.02} | 0.55 ^{+0.05} _{-0.03} |

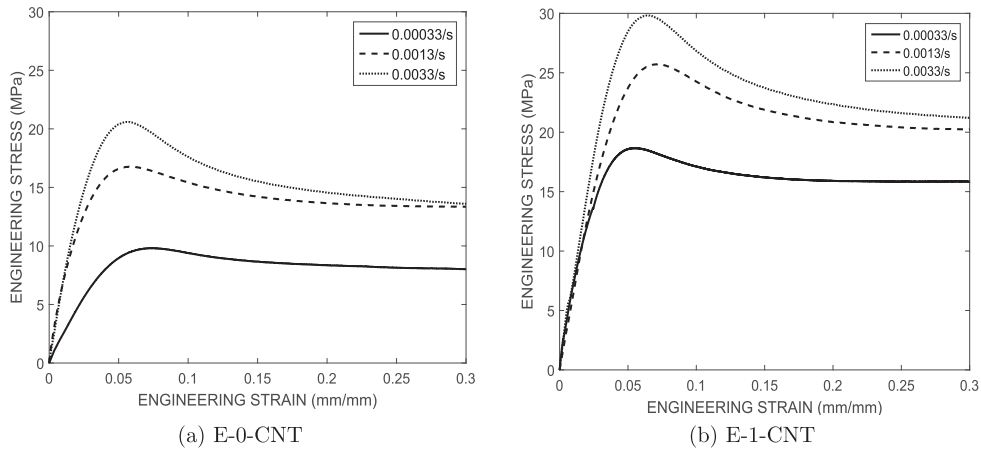


Fig. 3. Effect of Strain-Rate on the tensile properties.

Table 3
Tensile performance under different strain rates at room temperature.

| Property | Modulus (MPa) | | | Yield Strength (MPa) | | |
|----------|-------------------------------------|-------------------------------------|-------------------------------------|--------------------------------------|--------------------------------------|--------------------------------------|
| | 0.00033 | 0.0013 | 0.0033 | 0.00033 | 0.0013 | 0.0033 |
| E-0-CNT | 207.8 ⁺³⁵ ₋₄₆ | 450.2 ⁺¹³ ₋₂₁ | 521.5 ⁺¹⁴ ₋₂₅ | 9.8 ^{+1.3} _{-1.2} | 16.7 ^{+0.8} _{-1.8} | 20.5 ^{+1.5} _{-0.3} |
| E-1-CNT | 522.7 ⁺²⁷ ₋₁₂ | 616.2 ⁺³⁴ ₋₃₆ | 714.8 ⁺³⁰ ₋₄₂ | 18.6 ^{+1.4} _{-1.3} | 25.7 ^{+1.8} _{-1.1} | 29.8 ^{+1.5} _{-1.0} |

surface of the samples were analyzed. The studied samples were fractured in room temperature at a strain rate of 0.0013/s. The fractography of neat epoxy shows a relatively smooth fracture surface indicating a ductile failure mode. Fig. 7 shows the fracture surface of the nanocomposites at two different magnifications. At low magnifications a considerable difference in fracture surface can be observed. The depth in the river-bed pattern increases with the

increase in MWCNT content indicating a decrease in ductility of the nanocomposites. Even at low filler content, agglomerations can be observed as bright white spots in the low magnification micrographs. The size and concentration of agglomerations increase with the increase in MWCNT content with a corresponding decrease in failure strain and ductility [40]. Though the agglomerations are unavoidable due to the prolonged curing time at room

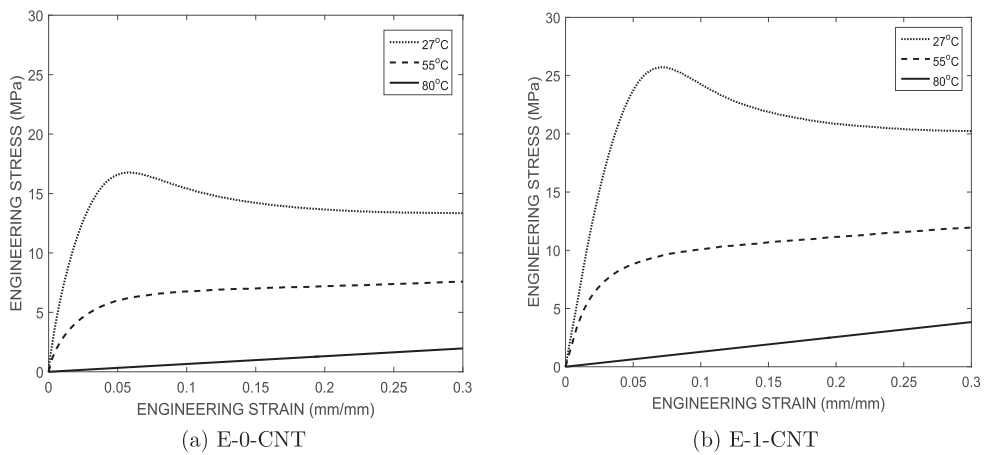


Fig. 4. Effect of Temperature on the tensile properties.

Table 4
Tensile performance under different temperatures at fixed strain rate.

| Property | Modulus (MPa) | | | Yield Strength (MPa) | | |
|----------|-------------------------------------|--------------------------------------|--------------------------------------|--------------------------------------|--------------------------------------|-------|
| | 27 °C | 55 °C | 80 °C | 27 °C | 55 °C | 80 °C |
| E-0-CNT | 450.2 ⁺¹³ ₋₂₁ | 206.9 ⁺²³ ₋₃₄ | 6.5 ^{+1.4} _{-0.5} | 16.7 ^{+0.8} _{-1.8} | 5.29 ^{+1.7} _{-0.9} | — |
| E-1-CNT | 616.2 ⁺³⁴ ₋₃₆ | 331.27 ⁺²⁴ ₋₄₀ | 12.8 ^{+1.3} _{-0.8} | 25.7 ^{+1.8} _{-1.1} | 7.39 ^{+1.3} _{-0.7} | — |

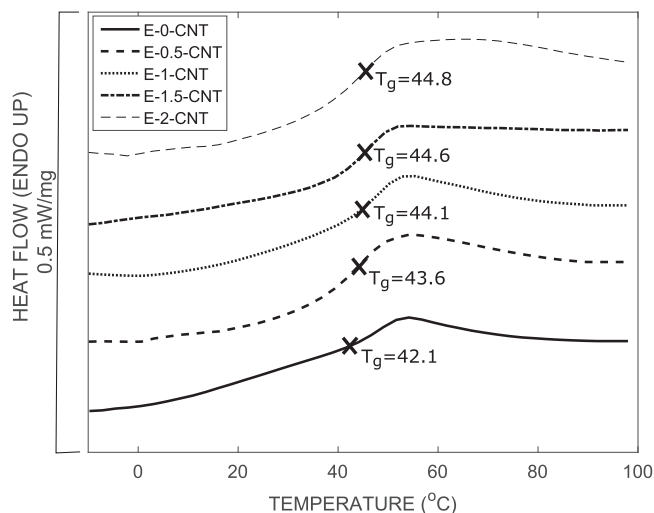


Fig. 5. DSC heating curves of the studied samples.

temperature, the average size of the agglomerates is found to be less than 1 μm and are uniformly distributed. The inset images show enlarged micro-graph of an agglomerate in respective nanocomposites.

The high magnification micro-graphs in Fig. 7 show individually pulled out MWCNTs protruding from the fracture surface. Wong et al. [41] studied the physical interactions of nanotube and polymer interface for epoxy and polystyrene matrices. They showed that these polymers adhered well to CNT surface at a nanometer scale due to electrostatic and Van-der-Waals forces resulting in a higher inter-facial shear strength which was about an order of magnitude higher than the composite. As seen in Fig. 7 all nanotubes including agglomerated MWCNTs are completely covered by epoxy indicating a good adhesion between MWCNT and the matrix

resulting in better mechanical properties. The average effective fiber diameter of epoxy coated MWCNT is found to be 85 nm.

3.4. Crystallographic properties

Fig. 8 shows the XRD patterns of MWCNT, epoxy and the nanocomposites. According to Bragg's law the location of the peak is important than the intensity of the peak, hence a constant intensity value was added to individual patterns in order to differentiate the XRD curves of various samples. It is seen that the pattern of MWCNT exhibits the characteristic sharp peak around $2\theta = 26^\circ$ and a short peak around $2\theta = 43^\circ$ relating to the interlayer spacing of nanotubes d_{002} and d_{100} reflections of C atoms [42]. For pure epoxy a broad peak can be observed around $2\theta = 19^\circ$ indicating the amorphous structure of epoxy. The XRD patterns of the studied nanocomposites show predominantly an amorphous structure. The characteristic diffraction peaks of MWCNT can be observed in the form of a slight shoulder in the pattern of E-2-CNT.

3.5. RPSM properties

The reversible plasticity shape memory effect of the nanocomposites was characterized within a strain limit of 30%. Though neat epoxy and nanocomposites with low filler content can exhibit RPSM characteristics at much higher strain levels, 30% strain was chosen in order to uniformly compare all samples and to avoid inflicting any permanent damages to nanocomposites with higher MWCNT content. Fig. 9 shows the effect of MWCNT reinforcement on the RPSM properties of epoxy nanocomposites under a constant strain-rate (0.0013/s), stress relaxation time (1800 s) and deformation strain (30%). It is observed that under the given conditions all samples show excellent shape memory properties. Though the samples have deformed to very high strains, the strain recovery of all samples are 100% when heated above T_g . In the thermo-mechanical tests conducted by Li and Xu [10] it was reported

Table 5

Linear Coefficient of Thermal Expansion (LCTE) and glass transition temperature (T_g) of different samples.

| Sample | LCTE below T_g ($10^{-5}/^\circ\text{C}$) | LCTE above T_g ($10^{-5}/^\circ\text{C}$) | T_g ($^\circ\text{C}$) (from DSC curves) |
|-----------|---|---|--|
| E-0-CNT | $6.04^{+0.7}_{-0.1}$ | $18.92^{+1.6}_{-0.4}$ | $42.1^{+1.0}_{-1.2}$ |
| E-0.5-CNT | $5.84^{+0.5}_{-0.4}$ | $18.16^{+0.8}_{-1.2}$ | $43.6^{+1.4}_{-2.0}$ |
| E-1-CNT | $5.97^{+0.3}_{-0.7}$ | $18.67^{+1.4}_{-1.0}$ | $44.1^{+1.5}_{-2.0}$ |
| E-1.5-CNT | $5.72^{+0.9}_{-0.3}$ | $18.79^{+1.7}_{-1.0}$ | $44.6^{+1.3}_{-1.6}$ |
| E-2-CNT | $5.56^{+0.2}_{-0.7}$ | $17.67^{+0.7}_{-0.9}$ | $44.8^{+1.6}_{-1.8}$ |

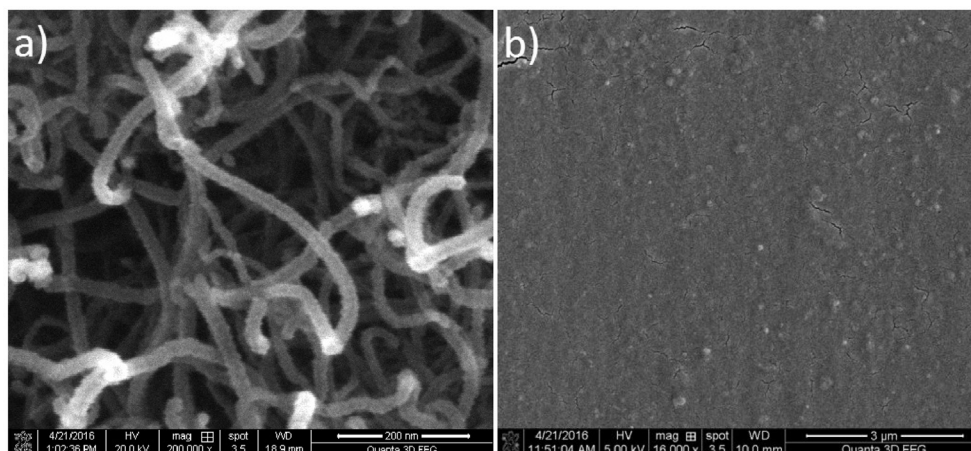


Fig. 6. FESEM micrographs of a)pristine MWCNT and b)fracture-surface of pure Epoxy, fractured at a strain rate of 0.0013/s in room temperature.

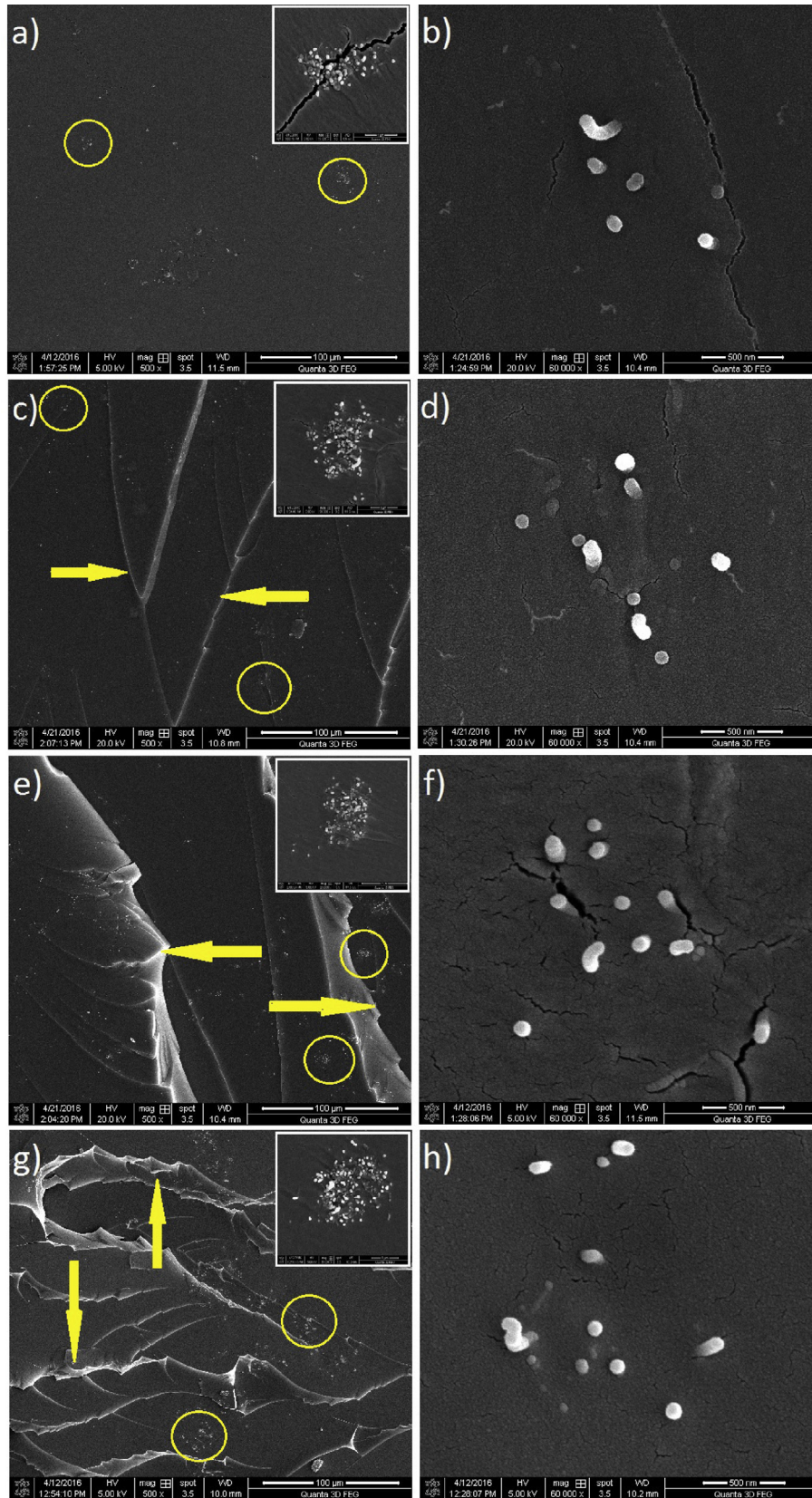


Fig. 7. FESEM micro-graphs of fracture-surface of E-0.5-CNT(a,b), E-1-CNT(c,d), E-1.5-CNT(e,f) and E-2-CNT(g,h) under different magnifications. All samples were fractured at a strain rate of 0.0013/s in room temperature. Fig. a,c,e and g are low magnification images (500 \times zoom) and Fig. b,d,f and h are high magnification images (60000 \times zoom). Arrows and circles indicate river-bed pattern and agglomerations respectively. Inset: Enlarged (35000 \times zoom) image of an agglomerate in respective nanocomposites.

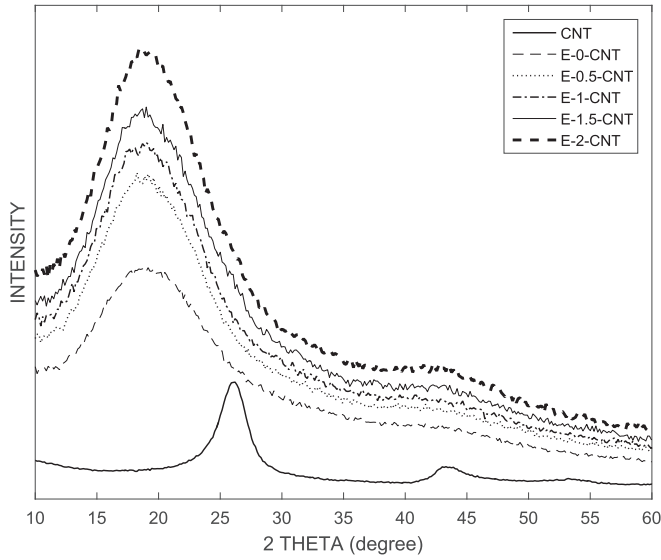


Fig. 8. XRD patterns of MWCNT, Epoxy and Nanocomposites.

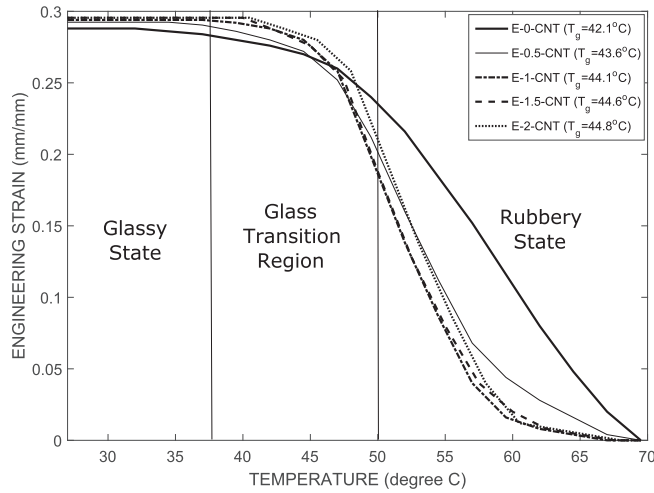


Fig. 9. Unconstrained strain recovery curves of the studied nanocomposites. Showing the Glassy state ($<T_g - 5$), Transition region ($T_g - 5$ to $T_g + 5$) and the Rubbery state ($>T_g + 5$).

that, at large deformations some permanent irreversible damage occurred with a programming temperature of $T_g - 42$ °C. In our experiments the deformation temperature is $T_g - 15$ °C where little or no irreversible damage have occurred during the cold drawing step. The benefit of MWCNT reinforcement is shown in Table 6 through three important shape memory parameters, namely; Shape Fixity (R_f), Response temperature (T_{res}) and Recovery speed (V_r). Shape fixity defines the ability of the material to hold a temporary shape. The temperature at which 50% of strain recovery has occurred is denoted by T_{res} . The recovery speed defines the

sensitivity of the material with temperature change and can be expressed as follows [43,44],

$$V_r = \frac{0.8R_f \epsilon_f \dot{T}}{T_{90} - T_{10}}$$

Where, T_{90} and T_{10} are temperatures corresponding to 90% and 10% strain recovery, respectively.

There is an improvement in the strain fixity with an increase in MWCNT content. The plastic deformation is fixed through the reorganization of segments which is held by the decreased segmental mobility in glassy state [5]. The improvement in fixity can be attributed to a further decrease in segmental mobility in the glassy state with the addition of MWCNT in the polymer matrix. The stress levels of the nanocomposites are higher throughout the thermo-mechanical cycle indicating an efficient reinforcement of MWCNT in the epoxy matrix. It has been reported [7,45] that the strain recovery starts at temperatures below T_g when the programming temperature is below T_g . A similar trend is observed in the present study for neat epoxy. This might be attributable to the increase in segmental mobility with an increase in temperature which would have enabled the material to recover. In E-0-CNT, the recovery has occurred over a range of temperature starting well before the glass transition and achieving a complete recovery well above T_g . This is not observed in nanocomposites where the recovery begins only after the temperature has reached T_g and the stored strain is recovered completely just above T_g as shown in Fig. 9. This indicates that the MWCNTs are able to successfully hold the fixed strain by restraining the segmental mobility until the temperature reaches T_g . Once the nanocomposite reaches rubbery state the material starts to recover under entropic elasticity of the matrix, assisted by the elastic energy stored in the MWCNT resulting in a higher recovery speed and a lower response temperature.

Fig. 10 shows a representative three-dimensional curve depicting the steps involved in a RPSM cycle and the macro-photographs of samples after various steps. The three dimensional plots distinctly show the following steps; i) loading step: loading at a constant strain rate up to a predetermined strain ($\sigma_0, \epsilon_0, t_0$), ii) relaxation step: the strain is kept constant until the stress reaches an asymptotic value ($\sigma_1, \epsilon_1 = \epsilon_0, t_1$), iii) unloading step: the load is removed instantly ($\sigma_2 = 0, \epsilon_2, t_2 = t_1$) and iv) strain recovery step: the sample is heated to a temperature higher than T_g at a constant heating rate where the sample recovers completely ($\sigma_3 = 0, \epsilon_3 = 0, t_3$). Fig. 11 shows the effect of strain rate on the RPSM properties of neat and MWCNT reinforced epoxy. The significance of strain rate can be observed in the relaxation curves. The time taken to reach ϵ_0 increases and the time taken to relax from σ_0 to σ_1 decreases i.e the time taken for the stress to reach an asymptotic value decreases. In E-0-CNT, there is no significant difference in the asymptotic value of the stress under different strain rates. Whereas, in E-1-CNT when the strain rate decreases the asymptotic value of the stress increases significantly i.e. when loaded at low strain rates MWCNT reinforced epoxy nanocomposite samples exhibit lesser stress relaxation than the samples which are loaded at high strain rates.

Table 6
RPSM performance of different samples.

| Parameter | E-0-CNT | E-0.5-CNT | E-1-CNT | E-1.5-CNT | E-2-CNT |
|----------------|--|--|--|--|--|
| R_f (%) | 96.4 ^{+0.5} _{-2.9} | 97.5 ^{+1.1} _{-2.1} | 98 ^{+0.6} _{-1.5} | 98.5 ^{+0.3} _{-1.3} | 98.5 ^{+0.3} _{-1.0} |
| T_{res} (°C) | 57.6 ^{+3.1} _{-1.1} | 52.5 ^{+1.8} _{-1.1} | 51.2 ^{+1.2} _{-3.4} | 51.1 ^{+1.0} _{-3.0} | 50.7 ^{+1.1} _{-3.6} |
| V_r (%/min) | 3.67 ^{+0.34} _{-0.39} | 4.58 ^{+0.68} _{-0.19} | 6.06 ^{+0.44} _{-0.40} | 6.08 ^{+0.58} _{-0.63} | 6.11 ^{+0.71} _{-0.67} |

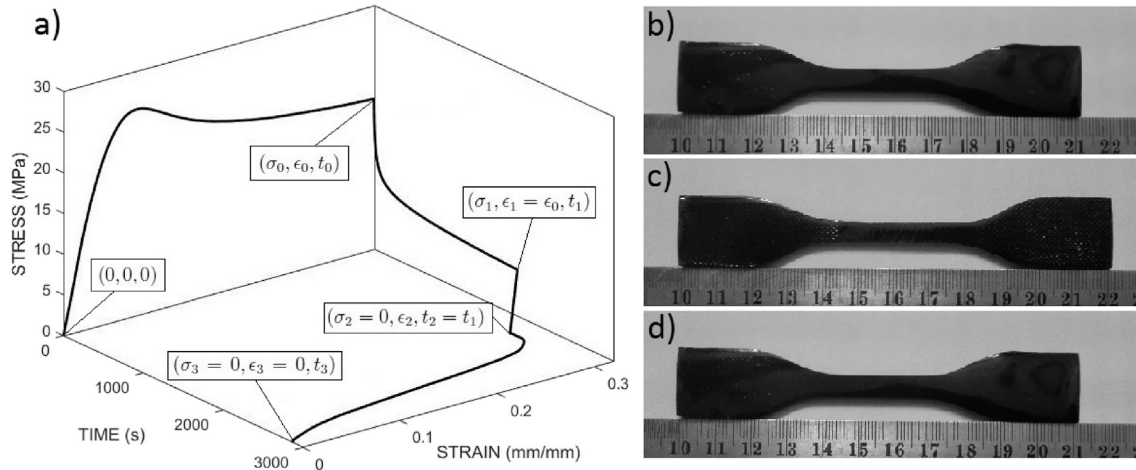


Fig. 10. a) Representative 3D plot showing the steps involved in a RPSM cycle. b) As prepared sample (E-1-CNT)–Permanent Shape c) After cold drawing and stress relaxation–Temporary Shape d) After stress-free recovery–Recovered Shape.

A possible explanation can be given as follows, at low strain rates an effective load transfer between MWCNT and the matrix might have occurred with minimal inter-facial failure enabling the MWCNTs to store the stress as elastic energy, leading to a lower stress relaxation.

Fig. 12 shows the effect of deformation length on the RPSM properties of E-0-CNT and E-1-CNT. The samples were tested for RPSM properties at three different strain levels namely; 10, 20 and 30%. Below 10%, for example at 5% strain level the deformation is predominantly in the elastic region, hence little or no strain fixity is observed regardless of the relaxation time for both neat and reinforced epoxy. It can be observed that the σ_0 value decreases as the deformation length increases, due to strain softening of the tensile specimen during cold drawing. This decrease in σ_0 ultimately leads to a decrease in the asymptotic value (σ_1). Once the deformation crosses onto inelastic region all samples show a decent amount of shape fixity. The pre-strain value has a considerable effect on the shape fixity at zero relaxation time, with an increase in pre-strain leading to an increase in shape fixity. No significant effect is observed in shape fixity when the samples are allowed to relax until the stress reaches an asymptotic value. So it can be concluded that good shape fixity can be

obtained for samples that have been deformed above the yield strain, if the samples are allowed to relax until the stress reaches an asymptotic value. To understand the effect of stress relaxation on RPSM properties the samples were tested for four relaxation times namely; 0, 5, 10 and 30 min and the results are presented in Fig. 13. It can be observed that with an increase in stress relaxation time a significant improvement in shape fixity can be obtained. For example the shape fixity in neat epoxy after relaxation times of 0, 5, 10 and 30 min is 85.2%, 88.1%, 94% and 96% respectively. It should be noted the shape fixity reaches a saturation value above which no amount of relaxation time will improve the shape fixity. Also, unlike conventional programming, 100% shape fixity cannot be obtained by cold drawing because a certain amount of strain is always instantaneously recovered during elastic unloading. For all relaxation times the shape fixity in nanocomposites were higher than neat epoxy. Also, since stress relaxation is a characteristic of the matrix, it has qualitatively similar effect on the nanocomposites.

The RPSM mechanism can be explained as follows; When the material is deformed beyond the initial yield, the molecular segments are reorganized which subsequently change its configurational entropy (Step i). In the glassy state (below T_g) the plastic

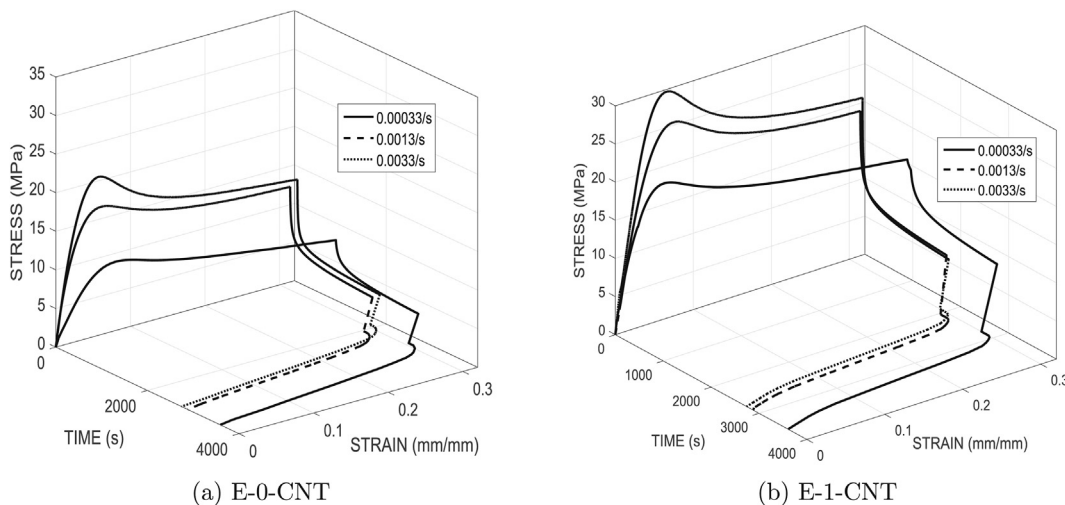


Fig. 11. Effect of strain-rate on the RPSM properties of a)E-0-CNT and b)E-1-CNT.

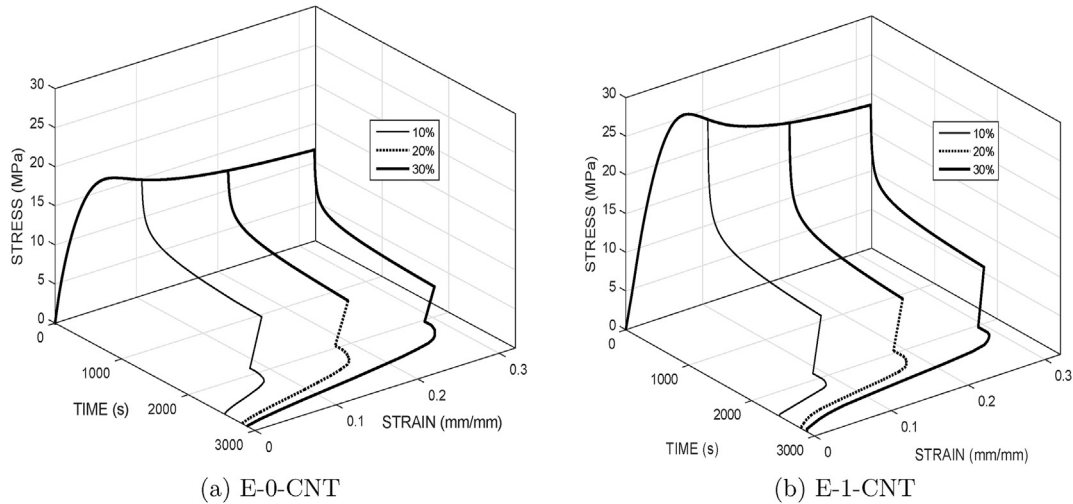


Fig. 12. Effect of deformation strain on the RPSM properties of a)E-0-CNT and b)E-1-CNT.

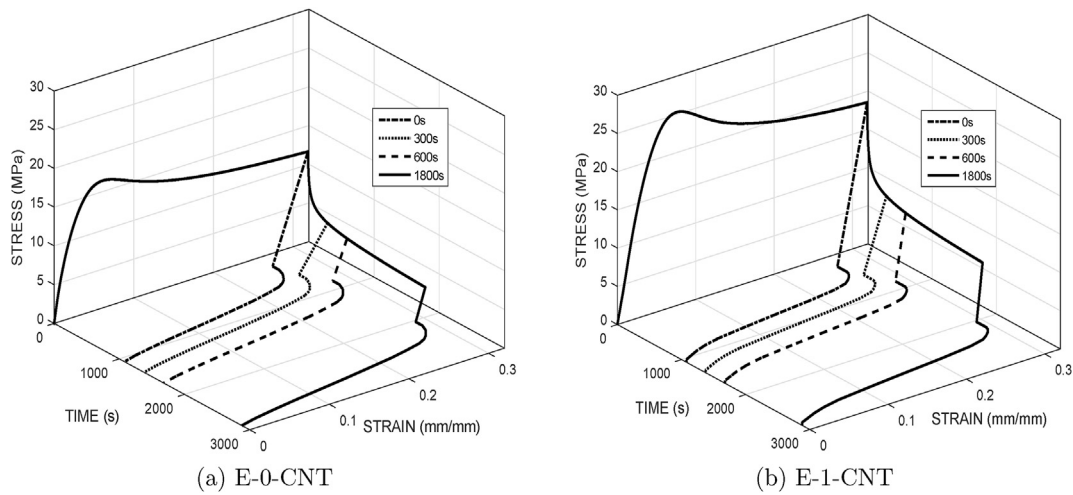


Fig. 13. Effect of relaxation time on the RPSM properties of a)E-0-CNT and b)E-1-CNT.

deformation is a rate-dependent process, so the relaxation time allows some reorientation of the deformed molecular structure where the stress reduces asymptotically to a non-zero value (Step ii). When the material is elastically unloaded, a relaxed stress-free configuration is obtained. The plastic deformation is fixed due to the high material viscosity and reduced segmental mobility in the glassy state (Step iii). When the sample is heated above T_g , the segmental mobility increases and the material recovers back to its original configuration driven by the entropic elasticity of the rubbery state (Step iv). This mechanism has been effectively captured using a thermo-viscoelastic-viscoplastic model proposed by Nguyen et al. [46] and the results are presented elsewhere [47].

From the above results and discussions it can be observed that by varying the different parameters like MWCNT content, transition region and programming conditions the material can be effectively designed as per requirements. For instance, in a self healing system, given the loading conditions like strain rate, the MWCNT content and the transition region can be optimized to ensure that the maximum strain is below the failure strain and that the plastic deformation is completely recovered. Likewise in an actuator or a morphing system, given the recovery conditions like morphing

configuration (recovery strain) and work to be done during actuation (recovery stress), the parameters can be effectively tuned to obtain the desired results.

4. Conclusion

In conclusion, an epoxy based SMP was tailored in order to achieve reversible plasticity shape memory properties. The properties of SMP was further improved by addition of multi-walled carbon nanotubes. The nanocomposites have been characterized for mechanical, thermal, morphological and crystallographic properties and the results were discussed. All samples showed excellent RPSM properties. The effect of MWCNT content and programming conditions like strain rate, deformation level and stress relaxation on the RPSM effect were studied systematically. The results proved that the addition of MWCNTs in the epoxy matrix significantly increases the mechanical and RPSM properties like improved shape fixity, response temperature and recovery speed. The results also show that the material is able to display RPSM effect under various programming conditions with 100% strain recovery in each case. This work also shows that by optimizing the parameters like MWCNT content and glass transition region, the

material can be effectively designed for applications in smart structures.

References

- [1] A. Lendlein, S. Kelch, Shape-memory polymers, *Angew. Chem. Int. Ed.* 41 (12) (2002) 2034–2057.
- [2] J. Hu, Y. Zhu, H. Huang, J. Lu, Recent advances in shape–memory polymers: structure, mechanism, functionality, modeling and applications, *Prog. Polym. Sci.* 37 (12) (2012) 1720–1763.
- [3] Tanpitaksit, T.; Jubsilp, C.; Rimdisut, S., Effects of benzoxazine resin on property enhancement of shape memory epoxy: a dual function of benzoxazine resin as a curing agent and a stable network segment. *Express Polym. Lett.*, 9(9).
- [4] T. Xie, Recent advances in polymer shape memory, *Polymer* 52 (22) (2011) 4985–5000.
- [5] X. Zhang, Z. Tang, B. Guo, Reversible plasticity shape memory polymers: key factors and applications, *J. Polym. Sci. Part B Polym. Phys.* 54 (14) (2016) 1295–1299.
- [6] C.M. Yakacki, S. Willis, C. Luders, K. Gall, Deformation limits in shape-memory polymers, *Adv. Eng. Mater.* 10 (1–2) (2008) 112–119.
- [7] K. Gall, C.M. Yakacki, Y. Liu, R. Shandas, N. Willett, K.S. Anseth, Thermo-mechanics of the shape memory effect in polymers for biomedical applications, *J. Biomed. Mater. Res. Part A* 73 (3) (2005) 339–348.
- [8] D.M. Feldkamp, I.A. Rousseau, Effect of the deformation temperature on the shape-memory behavior of epoxy networks, *Macromol. Mater. Eng.* 295 (8) (2010) 726–734.
- [9] N. Lakhera, C.M. Yakacki, T. Nguyen, C.P. Frick, et al., Partially constrained recovery of (meth) acrylate shape-memory polymer networks, *J. Appl. Polym. Sci.* 126 (1) (2012) 72–82.
- [10] G. Li, W. Xu, Thermomechanical behavior of thermoset shape memory polymer programmed by cold-compression: testing and constitutive modeling, *J. Mech. Phys. Solids* 59 (6) (2011) 1231–1250.
- [11] E.D. Rodriguez, X. Luo, P.T. Mather, Linear/network poly (*ε*-caprolactone) blends exhibiting shape memory assisted self-healing (smash), *ACS Appl. Mater. Interfaces* 3 (2) (2011) 152–161.
- [12] E. Wornyo, K. Gall, F. Yang, W. King, Nanoindentation of shape memory polymer networks, *Polymer* 48 (11) (2007) 3213–3225.
- [13] X. Xiao, T. Xie, Y.-T. Cheng, Self-healable graphene polymer composites, *J. Mater. Chem.* 20 (17) (2010) 3508–3514.
- [14] G. Li, O. Ajisafe, H. Meng, Effect of strain hardening of shape memory polymer fibers on healing efficiency of thermosetting polymer composites, *Polymer* 54 (2) (2013) 920–928.
- [15] G. Li, N. Uppu, Shape memory polymer based self-healing syntactic foam: 3-d confined thermomechanical characterization, *Compos. Sci. Technol.* 70 (9) (2010) 1419–1427.
- [16] J. Nji, G. Li, A biomimic shape memory polymer based self-healing particulate composite, *Polymer* 51 (25) (2010) 6021–6029.
- [17] L. Sun, W.M. Huang, Z. Ding, Y. Zhao, C.C. Wang, H. Purnawali, C. Tang, Stimulus-responsive shape memory materials: a review, *Mater. Des.* 33 (2012) 577–640.
- [18] J.H. Koo, *Polymer Nanocomposites*, McGraw-Hill Professional Pub, 2006.
- [19] E.T. Thostenson, T.-W. Chou, Processing-structure-multi-functional property relationship in carbon nanotube/epoxy composites, *Carbon* 44 (14) (2006) 3022–3029.
- [20] R. Velmurugan, T. Mohan, Room temperature processing of epoxy-clay nanocomposites, *J. Mater. Sci.* 39 (24) (2004) 7333–7339.
- [21] R. Velmurugan, T. Mohan, Epoxy-clay nanocomposites and hybrids: synthesis and characterization, *J. Reinf. Plast. Compos.* 28 (1) (2009) 17–37.
- [22] E.T. Thostenson, Z. Ren, T.-W. Chou, Advances in the science and technology of carbon nanotubes and their composites: a review, *Compos. Sci. Technol.* 61 (13) (2001) 1899–1912.
- [23] Q.-Q. Ni, C.-S. Zhang, Y. Fu, G. Dai, T. Kimura, Shape memory effect and mechanical properties of carbon nanotube/shape memory polymer nanocomposites, *Compos. Struct.* 81 (2) (2007) 176–184.
- [24] N.G. Sahoo, Y.C. Jung, H.J. Yoo, J.W. Cho, Influence of carbon nanotubes and polypyrrole on the thermal, mechanical and electroactive shape-memory properties of polyurethane nanocomposites, *Compos. Sci. Technol.* 67 (9) (2007) 1920–1929.
- [25] S. Hashmi, H.C. Prasad, R. Abishera, H.N. Bhargava, A. Naik, Improved recovery stress in multi-walled-carbon-nanotubes reinforced polyurethane, *Mater. Des.* 67 (2015) 492–500.
- [26] T. Gong, W. Li, H. Chen, L. Wang, S. Shao, S. Zhou, Remotely actuated shape memory effect of electrospun composite nanofibers, *Acta Biomater.* 8 (3) (2012) 1248–1259.
- [27] Y. Dong, H. Xia, Y. Zhu, Q.-Q. Ni, Y. Fu, Effect of epoxy-graft-polyoxyethylene octyl phenyl ether on preparation, mechanical properties and triple-shape memory effect of carbon nanotube/water-borne epoxy nanocomposites, *Compos. Sci. Technol.* 120 (2015) 17–25.
- [28] H. Koerner, G. Price, N.A. Pearce, M. Alexander, R.A. Vaia, Remotely actuated polymer nanocomposites/stress-recovery of carbon-nanotube-filled thermo-plastic elastomers, *Nat. Mater.* 3 (2) (2004) 115–120.
- [29] Y. Liu, H. Lv, X. Lan, J. Leng, S. Du, Review of electro-active shape-memory polymer composite, *Compos. Sci. Technol.* 69 (13) (2009) 2064–2068.
- [30] Y. Xiao, S. Zhou, L. Wang, T. Gong, Electro-active shape memory properties of poly (*ε*-caprolactone)/functionalized multiwalled carbon nanotube nanocomposite, *ACS Appl. Mater. Interfaces* 2 (12) (2010) 3506–3514.
- [31] W. Wang, D. Liu, Y. Liu, J. Leng, D. Bhattacharyya, Electrical actuation properties of reduced graphene oxide paper/epoxy-based shape memory composites, *Compos. Sci. Technol.* 106 (2015) 20–24.
- [32] T. Xie, I.A. Rousseau, Facile tailoring of thermal transition temperatures of epoxy shape memory polymers, *Polymer* 50 (8) (2009) 1852–1856.
- [33] C. Chui, M.C. Boyce, Monte carlo modeling of amorphous polymer deformation: evolution of stress with strain, *Macromolecules* 32 (11) (1999) 3795–3808.
- [34] P. Tordjeman, L. Teze, J. Halary, L. Monnerie, On the plastic and viscoelastic behavior of methylmethacrylate-based random copolymers, *Polym. Eng. Sci.* 37 (10) (1997) 1621–1632.
- [35] K. Chen, K.S. Schweizer, Theory of yielding, strain softening, and steady plastic flow in polymer glasses under constant strain rate deformation, *Macromolecules* 44 (10) (2011) 3988–4000.
- [36] S. Gurusideswar, R. Velmurugan, Strain rate sensitivity of glass/epoxy composites with nanofillers, *Mater. Des.* 60 (2014) 468–478.
- [37] A. Allaoui, N.-E. El Bounia, How carbon nanotubes affect the cure kinetics and glass transition temperature of their epoxy composites?—a review, *Express Polym. Lett.* 3 (9) (2009) 588–594.
- [38] P. Schelling, P. Keblinski, Thermal expansion of carbon structures, *Phys. Rev. B* 68 (3) (2003) 035425.
- [39] K. Shirasu, G. Yamamoto, I. Tamaki, T. Ogasawara, Y. Shimamura, Y. Inoue, T. Hashida, Negative axial thermal expansion coefficient of carbon nanotubes: experimental determination based on measurements of coefficient of thermal expansion for aligned carbon nanotube reinforced epoxy composites, *Carbon* 95 (2015) 904–909.
- [40] A. Montazeri, N. Montazeri, Viscoelastic and mechanical properties of multi walled carbon nanotube/epoxy composites with different nanotube content, *Mater. Des.* 32 (4) (2011) 2301–2307.
- [41] M. Wong, M. Paramsothy, X. Xu, Y. Ren, S. Li, K. Liao, Physical interactions at carbon nanotube-polymer interface, *Polymer* 44 (25) (2003) 7757–7764.
- [42] Y. Saito, T. Yoshikawa, S. Bandow, M. Tomita, T. Hayashi, Interlayer spacings in carbon nanotubes, *Phys. Rev. B* 48 (3) (1993) 1907.
- [43] I.A. Rousseau, Challenges of shape memory polymers: a review of the progress toward overcoming smp's limitations, *Polym. Eng. Sci.* 48 (11) (2008) 2075–2089.
- [44] F. Li, X. Zhang, J. Hou, M. Xu, X. Luo, D. Ma, B.K. Kim, Studies on thermally stimulated shape memory effect of segmented polyurethanes, *J. Appl. Polym. Sci.* 64 (8) (1997) 1511–1516.
- [45] P. Ping, W. Wang, X. Chen, X. Jing, Poly (*ε*-caprolactone) polyurethane and its shape-memory property, *Biomacromolecules* 6 (2) (2005) 587–592.
- [46] T.D. Nguyen, H.J. Qi, F. Castro, K.N. Long, A thermoviscoelastic model for amorphous shape memory polymers: incorporating structural and stress relaxation, *J. Mech. Phys. Solids* 56 (9) (2008) 2792–2814.
- [47] R. Abishera, R. Velmurugan, K.V.N. Gopal, Reversible plasticity shape memory effect in epoxy/cnt Nanocomposites – a theoretical study, *Compos. Sci. Technol.* (2016) (submitted for publication).